RSC Advances

PAPER

View Article Online
View Journal | View Issue

Cite this: *RSC Adv.*, 2024, **14**, 23011

Enhanced photocatalytic removal of bromate in drinking water by Au/TiO_2 under ultraviolet light†

Ying Xu, [ab] Shuili Yu,*[ab] Cong Huang[c] and Zheng Xu[c]

Received 10th May 2024
Accepted 5th July 2024

DOI: 10.1039/d4ra03453h

rsc.li/rsc-advances

The photo-reduction of bromate (BrO_3^-) has attracted much attention due to the carcinogenesis and genotoxicity of BrO_3^- in drinking water. In this study, a heterojunction photocatalyst was developed by depositing Au nanoparticles (NPs) onto P25 TiO_2 NPs through a one-pot, solvent-thermal process. Due to the unique properties of Au, the Au NPs deposited on the TiO_2 surface created a Schottky barrier between the metal and the semiconductor, leading to an effective separation of photo-generated charge carriers as the Au nanoparticles served as electron sinks. The Au/TiO_2 photocatalyst demonstrated efficient reduction of BrO_3^- under UV light illumination without the need for sacrificial agents. The effect of different Au loading of Au/TiO_2 was systematically investigated for its influence on the generation of electrons and the reduction ability of BrO_3^-. The results indicate that the 1% Au/TiO_2 catalyst exhibited a higher concentration of localized electrons, rendering it more effective in BrO_3^- removal. The photocatalytic efficiency for BrO_3^- reduction decreased upon the addition of $K_2S_2O_8$ as an electron quencher, suggesting that the primary factor in this photo-reduction process was the availability of electrons. These findings hold promise for the potential application of the Au/TiO_2 catalyst in the removal of BrO_3^- from drinking water through photo-reduction.

1 Introduction

Bromate (BrO_3^-) is a common by-product of ozone oxidation or chlorination of bromine (Br^-) in water.[1–3] Br^- is ubiquitous, and its concentration range varies in different water bodies. Our group detected Br^- concentrations of ~170–200 μg L^{-1} in the East Tai Lake. Krasner *et al.* investigated Br^- in American rivers and found that the concentration of Br^- was ~10–3000 μg L^{-1}.[4] In seawater, Br^- was also present at levels up to 67 mg L^{-1}.[5] In addition, BrO_3^- is frequently used in industrial applications such as food additives and hair dyes, beer and cheese processing, gold extraction, wool production, and the production and use of sodium hypochlorite disinfectants. The widespread use of the ozone oxidation process and the direct discharge of pollutants from industrial applications have led to increasing concentrations of BrO_3^- in various water bodies.[6] Due to its carcinogenic and mutagenic effects on humans, BrO_3^- has been classified as a Group 2B carcinogen by the International Agency for Research on Cancer.[7] The World Health Organization (WHO) has limited its maximum contamination concentration to 10 μg L^{-1}.[8] The latest drinking water standards in the U.S., EU, and China also stipulate a BrO_3^- limit of 10 μg L^{-1}.[9]

The current methods to control and remove BrO_3^- mainly include mid-control methods to inhibit BrO_3^- formation and post-treatment methods to remove BrO_3^-.[10] Medium control methods to inhibit BrO_3^- formation include optimizing ozone dosing, optimizing reactors, increasing acidity to reduce pH, *etc.* However, these measures still cannot wholly avoid BrO_3^- production. Therefore, further BrO_3^- removal technologies are needed.[11–13] Activated carbon could remove BrO_3^- but is limited by the adsorption capacity of activated carbon.[14] Membrane treatment and ion exchange affect BrO_3^- removal, but they only play a separating role.[15] The iron reduction method can effectively remove BrO_3^-, but the iron ions generated by the reaction will produce secondary pollution, which is challenging to apply in practical water plants.[16]

In contrast to conventional removal methods, the photocatalytic degradation of BrO_3^- offers notable advantages such as high efficiency in removal and facile integration with the UV disinfection process employed in drinking water treatment facilities.[17] As a common photocatalyst, TiO_2 has attracted wide attention for its low price, non-toxicity, good stability, and high catalytic activity.[18–20] However, the wide band gap of TiO_2 leads to low light utilization, which increases the compounding rate of photo-generated electrons and holes. To address these challenges intelligently, a promising approach involves the modification of semiconductors with noble metal

[a]State Key Laboratory of Pollution Control and Resource Reuse, College of Environmental Science and Engineering, Tongji University, Shanghai 200092, P. R. China. E-mail: ysl@tongji.edu.cn

[b]Shanghai Institute of Pollution Control and Ecological Security, Shanghai 200092, P. R. China

[c]PowerChina Huadong Engineering Corporation Limited, Hangzhou 311122, P. R. China

† Electronic supplementary information (ESI) available. See DOI: https://doi.org/10.1039/d4ra03453h

nanoparticles, such as gold nanoparticles (Au NPs).[21–23] By grafting these nanoparticles onto the surface of the semiconductor, a heterojunction referred to as the Schottky barrier is formed between the metal and the semiconductor. This barrier facilitates the transfer of photo-generated electrons from the conduction band (CB) of the TiO_2 semiconductor to the plasmonic Au NPs, resulting in the efficient separation of charge carriers. The presence of Au NPs as electron sinks enhances the photocatalytic activity under UV light, thereby promoting the effective degradation of BrO_3^-.[24,25] Besides this, the application of Au/TiO_2 catalysts in BrO_3^- photoreduction is less reported.

In this study, a one-pot solvent-thermal method was successfully developed for synthesizing Au/TiO_2 heterojunction photocatalysts, which exhibited exceptional photo-reduction capabilities for BrO_3^- under UV irradiation without the need for additional sacrificial agents. The photo-reduction experiments of BrO_3^- using 1% Au/TiO_2 photocatalyst were carried out under UV light. In addition, the photo-reduction efficiency of the Au/TiO_2 photocatalyst for BrO_3^- was evaluated under different influencing factors, and the reusability and stability of the photocatalyst were investigated.

2 Materials and methods

2.1 Materials and chemicals

Non-porous TiO_2 nanoparticles with a size of 21 nm and a surface area of 50 $m^2\ g^{-1}$ (AEROXIDE TiO_2 P25, Evonik (Degussa), Germany) were utilized in the study. Sodium bromate, humic acid, and polyvinylpyrrolidone (PVP) with a molecular weight of 58 000 were procured from Aladdin Industrial Corporation (Shanghai, P.R. China). Tetrachloroauric (III) acid tetrahydrate, ethylene glycol, nitric acid, and ethanol were obtained from Sinopharm Chemical Reagent Corporation (Shanghai, P.R. China). All chemicals employed in the study were of analytical grade and were used without further purification. DI water with a resistivity of 18.2 MΩ cm, obtained from a Milli-Q system (Millipore), was used throughout the experimental procedures. A concentration of 10 mg L^{-1} of BrO_3^- samples was prepared by diluting a stock solution of 1 g L^{-1} in DI water. Tap water was collected from local water plants responsible for treating raw water from the Yangtze River, and it was utilized to evaluate the performance of Au/TiO_2 under UV irradiation. Detailed information regarding the significant characteristics of tap water is provided in Table S1 in the ESI (ESI).†

2.2 Synthesis of the Au/TiO_2 photocatalyst

The Au/TiO_2 photocatalyst was synthesized using a facile one-pot solvothermal method. At room temperature, 1 ml of nitric acid (10 M) and 9 ml of DI water were added to 50 ml of ethylene glycol while stirring. Then 0.05 g of tetrachloroauric (III) acid tetrahydrate, 1 g of polyvinylpyrrolidone, and 1 g of titanium dioxide (Degussa P25) were added to the above mixture, and the mixture was stirred and sonicated alternately at 15 min intervals. After thorough mixing, the mixture was transferred to 100 ml of Teflon-lined autoclaves and subjected to a solvent-thermal reaction temperature of 150 °C for 24 h. The precipitate was obtained by natural cooling to room temperature of 25 °C at the end of the reaction and was washed three times repeatedly with DI water and ethanol to obtain the final product of 1% Au/TiO_2 photocatalyst, where the molar ratio of Au/Ti was 1%. 0.5% Au/TiO_2 and 5% Au/TiO_2 photocatalyst were prepared by the same method, varying the additional amount of tetra chloroauric (III) acid tetrahydrate.

2.3 Characterization of the Au/TiO_2 photocatalyst

The X-ray powder pattern of the samples was obtained using an X-ray diffractometer (XRD, D8 Advance, Bruker Corp.) with Cu Ka radiation operating at a voltage of 40 kV and a current of 40 mA. Phase and crystallinity of the prepared samples were further explored by Raman spectroscopy (LabRAM HR Evolution, Horiba). The morphology of the samples was investigated using transmission electron microscopy (TEM, FEI, Tecnai G2 F20). The surface elemental compositions of the samples were analyzed using X-ray photoelectron spectroscopy (XPS, ESCALAB 250Xi, Thermo Fisher Scientific). The surface of photocatalysts was investigated by Fourier transform infrared spectroscopy (FTIR, Nicolet iS20, Thermo Nicolet Corp.). The UV-vis diffuse reflection spectra (UV-vis DRS) of the dry-pressed disk samples were recorded using a UV-vis spectrophotometer (UV-2550, Shimadzu). Photoluminescence spectra (PL) of the samples were acquired using a fluorescence spectrophotometer (FLS920, Edinburgh Instruments) equipped with a xenon lamp, with an excitation wavelength of 380 nm.

2.4 Photocatalytic reduction of BrO_3^- under UV illumination

In this study, the target contaminant investigated was BrO_3^-. The photoreactors and experimental methods for light exposure have been previously described and illustrated in Fig. S1.†,[9] The cylindrical photoreactor utilized had a volume (V) of 1.6 L, and the light source employed was a 15 W low-pressure mercury UV lamp (UV-L, Cnlight, China). In a typical experimental setup, a 50 ml aqueous solution of BrO_3^- (10 mg L^{-1}) was introduced into a cylindrical quartz tube reactor, along with 10 mg of the photocatalyst. All quartz tubes were positioned on a turntable that rotated around the UV lamp to ensure uniform exposure. Following the irradiation period, 5 ml of the suspension was collected at fixed sampling intervals, and the photocatalyst was separated through centrifugation at 10 000 r min^{-1} for 5 minutes. The resulting suspension was then filtered using a 0.22 μm Millipore syringe filter. The residual concentration of BrO_3^- in the supernatant was determined by ion chromatography (Dionex ICS 1000 ion chromatography). Each experiment was independently repeated at least three times, and the reported values represent the average with standard deviation.

3 Results and discussions

3.1 Characterization of Au/TiO_2 photocatalyst

Fig. 1(a) shows the XRD patterns of Au/TiO_2 photocatalysts with Au loading from 0% to 5%. It could be seen that all samples

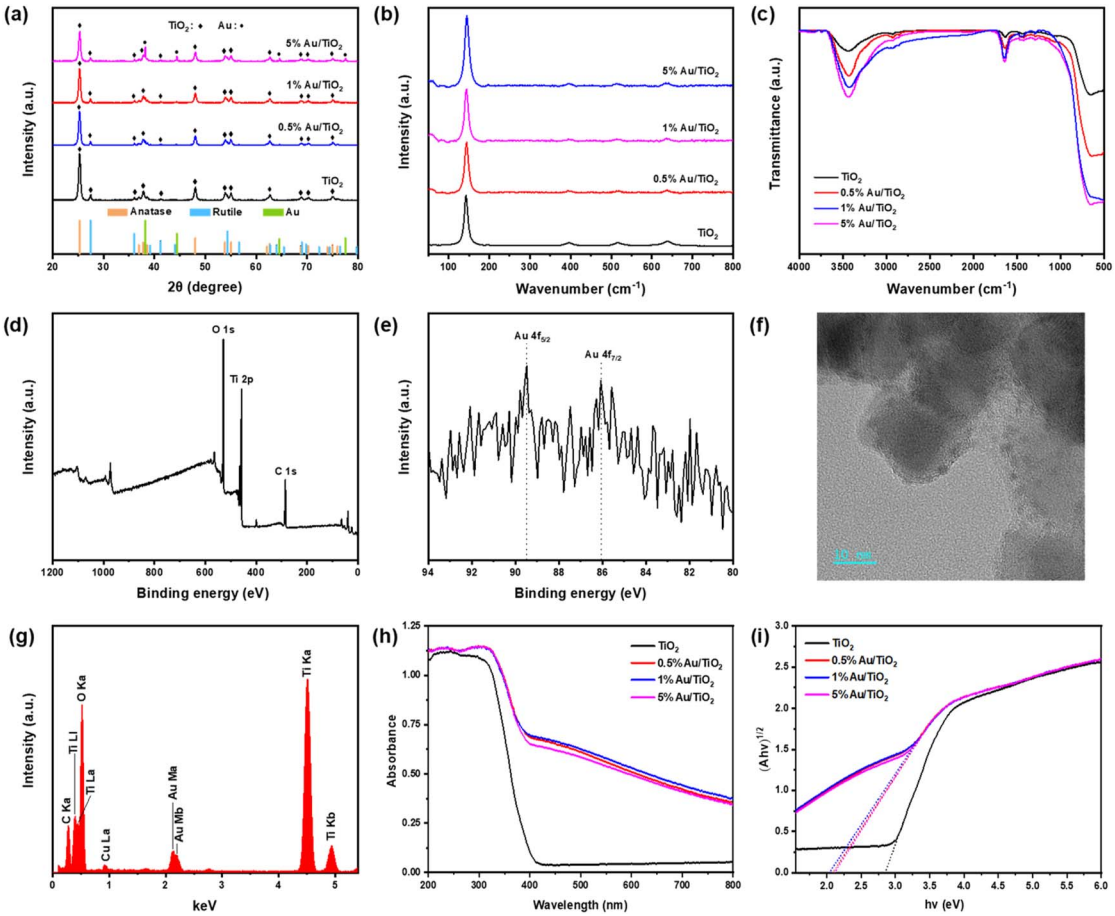

Fig. 1 (a) The XRD patterns, (b) Raman spectra and (c) FTIR spectra of the Au/TiO_2 photocatalyst. (d) XPS survey spectrum and (e) High-resolution XPS scans over the Au 4f peaks of the 1% Au/TiO_2 photocatalyst. (f) HRTEM image of the 1% Au/TiO_2 photocatalyst. (g) Energy dispersive spectrometer (EDS) spectra of the HRTEM image. (h) UV–vis diffuse reflectance spectra of TiO_2 and Au/TiO_2 photocatalyst. (i) Determination of band gaps of prepared photocatalyst using Tauc's method.

clearly showed the anatase and rutile phases of TiO_2 after the solvothermal reaction, which was consistent with the composition of Degussa P25 (~80% anatase and 20% rutile), indicating that the catalyst preparation process did not affect the phases of TiO_2 nanoparticles.[26,27] However, no significant XRD peaks for Au were observed when the molar ratio of Au/Ti was 0.5% and 1%, which may be attributed to the low concentration and very small agglomeration of Au NPs.[28] The Raman spectra of Au/TiO_2 photocatalysts exhibit characteristic peaks of TiO_2 at 144 cm^{-1} (E_g), 197 cm^{-1} (E_g), 399 cm^{-1} (B_{1g}), 513 cm^{-1} (A_{1g}), and 639 cm^{-1} (E_g) in Fig. 1(b).[29] Upon Au loading, the positions of these peaks remain unchanged, indicating the preservation of the TiO_2 crystalline structure. Notably, the intensity of the peak at 144 cm^{-1} (E_g) increases compared to pure TiO_2, suggesting an enhancement due to surface plasmon resonance effects from the Au nanoparticles.[30] However, other peak intensities decrease with increasing Au content, likely due to the coverage of TiO_2 surfaces by Au, which attenuates the Raman signal.[31] This analysis confirms that while Au incorporation influences specific vibrational modes, it does not disrupt the TiO_2 lattice.

The FTIR spectra reveal significant changes in TiO_2 with varying Au loadings (Fig. 1(c)). Pure TiO_2 exhibits characteristic Ti–O–Ti bending at ~450 cm^{-1} and O–H stretching around ~1630 cm^{-1} and ~3400 cm^{-1}.[32] With Au loading, these peaks show changes in intensity, indicating interactions between Au nanoparticles and TiO_2 surface groups, while the unchanged peak positions suggest the fundamental chemical structure remains intact. Higher Au loadings (5%) cause more pronounced changes in intensity, suggesting substantial modifications in surface adsorption properties and exposure of active sites on TiO_2.[33] The XPS survey spectra of the 1% Au/TiO_2 photocatalyst are presented in Fig. 1(d). The spectra display peaks corresponding to the O 1s, Ti 2p, and C 1s signals originating from oxygen, titanium, and carbon (from the carbon tape), respectively. However, no distinct Au spectra are observed in the survey spectrum. Further analysis using high-resolution XPS revealed two peaks at approximately 89.5 eV and 86.1 eV for the 1% Au/TiO_2 photocatalyst (Fig. 1(e)). These peaks are assigned to the spin components of Au $4f_{5/2}$ and Au $4f_{7/2}$, respectively. Additionally, the high-resolution XPS scan of the Ti 2p peaks, shown in Fig. S2,† indicates that Ti^{4+} is the dominant species in the photocatalyst.[34]

The HRTEM image of the 1% Au/TiO_2 photocatalyst is shown in Fig. 1(f). The average size of the P25 TiO_2 nanoparticles was

found to be approximately 20 nm, which is consistent with the existing findings.[35] The dark and extremely small NPs (2–3 nm) dispersed on the surface of TiO_2 are very likely Au NPs. The energy dispersive spectrometer spectrum (Fig. 1(f)) of the TEM image shown in Fig. 1(g) proves the existence of Bi together with Ti and O, verifying the successful loading of Au on TiO_2 NPs. The C and Cu signals are probably from the carbon film and the copper mesh of the TEM grid, respectively. Because Bi has a much higher atomic weight (197) than that of Ti (48) and O (16), Bi NPs would appear darker than TiO_2 under TEM. Furthermore, EDS mapping images in Fig. S3† also clearly showed the existence and distribution of Au, O, and Ti elements. ICP-MS measurement results showed that Au/Ti atomic ratio of 0.5% Au/TiO_2, 1% Au/TiO_2 and 5% Au/TiO_2 was about 0.45%, 0.97% and 4.8%, respectively, which was close to that in the preparation of the composites.

3.2 The UV absorbance of Au/TiO_2 photocatalyst

The light absorption performance of the Au/TiO_2 photocatalyst was probed by UV-vis diffuse reflection. As shown in Fig. 1(h), the light absorption capacity of the catalysts loaded with Au NPs was enhanced compared with that of pure TiO_2. In addition, the absorption spectra of the Au/TiO_2 photocatalyst showed a certain degree of a red-shift phenomenon, which might be attributed to the interaction between TiO_2 and Au NPs, thus reducing the energy required for electron leap.[36,37]

The band gaps (E_g) of the Au/TiO_2 photocatalyst were determined using Tauc's method, as described by eqn (1):

$$a(hv) = k(hv - E_g)^{n/2} \quad (1)$$

In the equation, α represents the absorption coefficient, h is the Planck constant, v is the light frequency, k is a proportionality constant, and n depends on the type of optical transition of the semiconductor ($n = 1$ for direct-band-gap and $n = 4$ for indirect-band-gap semiconductors). For TiO_2 NPs, the value of n is 4.[38] In this study, absorbance (A) was used instead of α in eqn (1). Since A is proportional to α, the band gap of the semiconductor can be estimated by determining the x-intercept when extrapolating the linear region in the absorption edge of the plot of $(Ahv)^{1/2}$ *vs.* hv, as shown in Fig. 1(i).[9] The band gaps of the 0.5% Au/TiO_2, 1% Au/TiO_2, and 5% Au/TiO_2 photocatalysts were found to be 2.08 eV, 2.03 eV, and 2.12 eV, respectively. These values are significantly narrower than that of TiO_2 (2.85 eV), indicating an enhancement in the photocatalytic reaction activity. The Au/TiO_2 photocatalyst exhibited a plasmonic absorption band at 530 nm, consistent with the presence of Au NPs.[39]

3.3 Photocatalytic reduction of BrO_3^- by the Au/TiO_2 photocatalyst

To investigate the performance of Au/TiO_2 photocatalyst for photo-reduction of BrO_3^-, the changes of BrO_3^- concentration were observed under the conditions of dark adsorption, UV alone, direct photo-reduction, and photo-reduction after adsorption (30 min), respectively.

The experimental results are shown in Fig. 2. It could be seen that the best performance of BrO_3^- removal was achieved by photo-reduction after adsorption (30 min), with 99% BrO_3^- removal at 60 minutes, while the BrO_3^- removal at 60 minutes was only 90% under the condition of direct photo-reduction without dark adsorption. Combined with the experimental results of the complete dark adsorption reaction, it could be concluded that the dark adsorption process can promote the photo-reduction process but has no significant effect on the removal of BrO_3^-. This might be attributed to the photo-reduction in this experiment as an interfacial reaction. The amount of BrO_3^- adsorbed by the photocatalyst after 60 min dark adsorption was about 5%. Meanwhile, the direct UV also affected BrO_3^- removal, but only 32% of BrO_3^- was removed in 60 min, which was not very satisfactory. Therefore, in the absence of special instructions, the experiments in this study were performed with photo-reduction after adsorption (30 min).

3.4 The effect of Au mass, bromate concentration, catalyst dosage, pH, temperature, humic acid, and O_2 concentration on the BrO_3^- reduction by Au/TiO_2 photocatalyst

Fig. 3(a) shows the degradation of BrO_3^- by Au/TiO_2 photocatalyst with different Au loadings under UV irradiation. In the presence of UV/TiO_2, the BrO_3^- removal was only 61% after 60 min, and 39% of BrO_3^- remained in the aqueous solution, which still poses a risk of BrO_3^- overload. In contrast, the photocatalytic activity of all Au/TiO_2 photocatalysts was higher compared to pure TiO_2. The removal rate of BrO_3^- exceeded 85% after 60 minutes of photocatalytic treatment. Among them, the 1% Au/TiO_2 photocatalyst showed the best BrO_3^- degradation with 99% at 60 min, followed by 0.5% Au/TiO_2 and 5% Au/TiO_2 with 92% and 87%, respectively. The presence of the Schottky barrier at the interface between the Au and TiO_2 facilitates the efficient transfer of photo-generated electrons

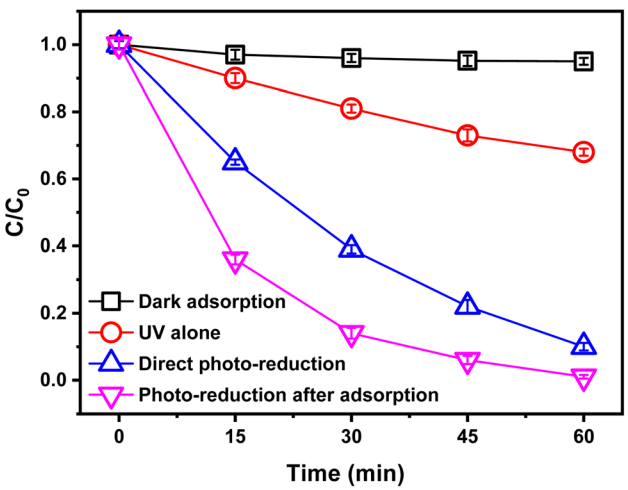

Fig. 2 Photo-reduction of BrO_3^- in dark adsorption, UV alone, direct photo-reduction, and photo-reduction after adsorption. Conditions: $[BrO_3^-]_0 = 0.078$ mM (10 mg L^{-1}), 1% Au/TiO_2 dose = 0.3 g L^{-1}, pH = 7.0 ± 0.2, DO = 8.1 mg L^{-1}, $T = 25 \pm 0.5$ °C, and UV-L light intensity = 2.42 mW cm^{-2}.

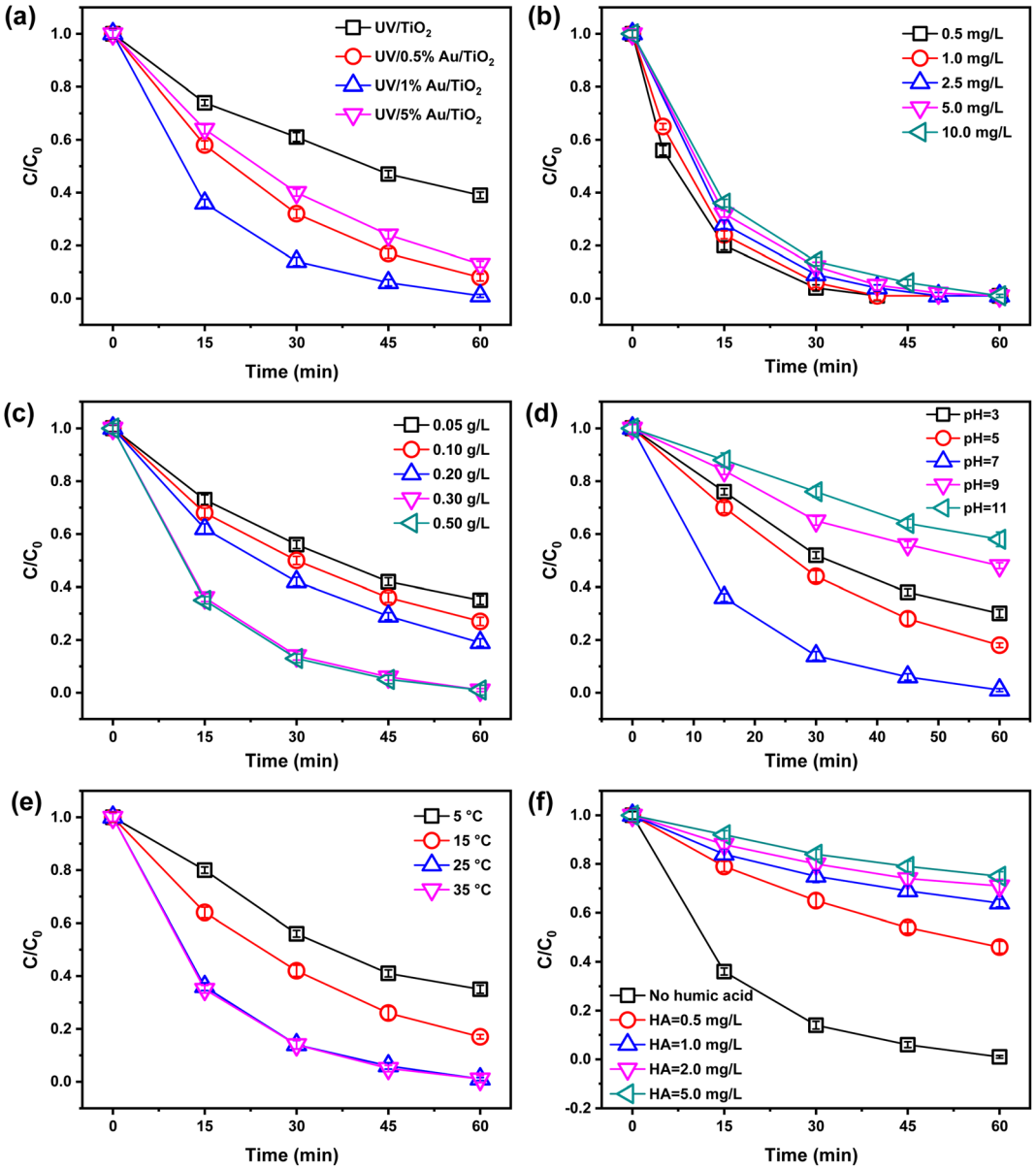

Fig. 3 Effects of (a) Au mass, (b) bromate concentration, (c) catalyst dosage, (d) pH, (e) temperature and (f) humic acid (HA) on the reduction of BrO_3^- by Au/TiO_2 photocatalyst. Conditions: Au mass = 1% unless varied in (a), $[BrO_3^-]_0$ = 0.078 mM (10 mg L^{-1}) unless varied in (b), catalyst dose = 0.3 g L^{-1} unless varied in (c), pH = 7.0 ± 0.2 unless varied in (d), T = 25 ± 0.5 °C unless varied in (e), DO = 8.1 mg L^{-1} and UV-L light intensity = 2.42 mW cm^{-2}.

from the conduction band (CB) of TiO_2 to the plasmonic Au NPs. This transfer process enables the effective separation of charge carriers, as the Au NPs can act as electron sinks. As expected, the increase of Au NPs in the composites did not improve the BrO_3^- degradation rate, suggesting that the Au loading has reached saturation. Too many Au NPs will agglomerate and cover the TiO_2 surface, reducing the surface area of TiO_2 exposed to UV irradiation, thus decreasing the photocatalytic activity of the catalyst.[40] Subsequently, the kinetics of the photo-reduction of BrO_3^- were analyzed and studied (Fig. S4†). The kinetics of the processes followed the pseudo-first-order kinetics equation, $\ln(C/C_0) = kt$, where C is the concentration of BrO_3^- at a given time, C_0 is the initial concentration of BrO_3^-, k is the apparent rate constant, and t is the reaction time. The calculated values of the apparent rate constant (k) are presented in Table S2.† The rate constant for the reduction of BrO_3^- using the 1% Au/TiO_2 photocatalyst was determined to be 0.0707 min^{-1}. This value is 4.34 times higher than that of commercial P25 TiO_2 (0.0163 min^{-1}), 1.74 times higher than that of 0.5% Au/TiO_2 (0.0405 min^{-1}), and 2.16 times higher than that of 5% Au/TiO_2 (0.0327 min^{-1}) (Table S2†). Based on this analysis, the 1% Au/TiO_2 photocatalyst was selected for further experiments.

The impact of initial BrO_3^- concentration (0.5 to 10 mg L^{-1}) on BrO_3^- removal efficiency was investigated, as shown in Fig. 3(b). The study indicates that using 1% Au/TiO_2 as

a photocatalyst, the degradation efficiency of BrO_3^- decreases with increasing initial concentration. This decline in efficiency is primarily due to the competition for active sites on the catalyst surface. As the BrO_3^- concentration rises, more molecules compete for the limited active sites, reducing the likelihood of each molecule interacting with the catalyst and thus lowering the overall degradation efficiency.[41]

The catalyst dosage not only affects the BrO_3^- degradation effect but also determines the economics of the whole photocatalytic reaction system. The degradation of BrO_3^- by 1% Au/TiO_2 photocatalyst with different dosages is shown in Fig. 3(c). The BrO_3^- removal rates at 60 min were 65%, 73%, 81%, 99%, and 99% for catalyst dosages of 0.05, 0.10 0.20, 0.30, and 0.50 g L^{-1}, respectively. When the 1% Au/TiO_2 dosage was increased from 0.3 to 0.5 g L^{-1}, the degradation of BrO_3^- was not significantly enhanced, indicating that the optimal catalyst dosage (0.3 g L^{-1}) occurred in the photo-reduction process. The high photocatalyst concentration at 0.5 g L^{-1} might induce more significant catalyst aggregation in the solution, resulting in lower BrO_3^- degradation. Moreover, it should be noted that using an excess solid-to-solution ratio can result in increased turbidity in the reaction system, which may lead to the scattering of light and hinder effective light penetration through the BrO_3^- solution.[42]

Fig. 3(d) depicted the impact of initial pH on the reduction of BrO_3^- in the UV/1% Au/TiO_2 process. The results indicated a significant dependency of BrO_3^-degradation on the pH value, with the highest removal rate observed at pH 7 after 60 minutes of reaction time. Too much H^+ or OH^- in the system would have a significant adverse effect on BrO_3^- photo-reduction. Compared with an acidic solution, an alkaline environment was more unfavorable to the degradation of BrO_3^-, which was mainly attributed to the competition between OH^- and BrO_3^- on the surface of the composite. For further investigation, the zeta potential of the 1% Au/TiO_2 catalyst was measured (Fig. S5†), and it was observed that the zeta potential became more negative as the initial pH increased. At pH 3, 5, 7, 9, and 11, the zeta potential values were 9.4 mV, 6.2 mV, −10.1 mV, −23.7 mV, and −28.4 mV, respectively. With decreasing pH, the functional groups on the catalyst surface became protonated, leading to an increased proportion of positively charged surfaces. Under alkaline conditions, the presence of anions and the negatively charged surface of the 1% Au/TiO_2 particles, adsorbed by OH–, resulted in repulsive effects. This led to reduced contact between BrO_3^- and the catalyst particles, resulting in lower photocatalytic activity.[43] Furthermore, it is worth mentioning that the reaction between OH^- and positive holes generated during the photocatalytic process led to the formation of hydroxyl radicals ($OH^\bullet$). These hydroxyl radicals played a crucial role in oxidizing Br^- to BrO_3^-, which is in line with previous findings and supports the proposed mechanism of the photocatalytic reaction.[44] As for acidic conditions, more electrons migrated to the surface of the catalyst due to their gravity, increasing the reduction efficiency. Indeed, excessive H^+ concentration can lead to the consumption of OH^- ions and facilitate the formation of highly oxidizing species such as hydroperoxyl radicals ($HO_2^\bullet$). These radicals can participate in the oxidation of bromide ions, resulting in the generation of BrO_3^-.[45] This also explained the low BrO_3^- degradation rate at PH ≤ 5, mainly due to the loss of electrons and the formation of oxidizing radicals.[46]

In this study, the effect of temperature on BrO_3^- removal was investigated over a range of 5 °C to 35 °C. The results, shown in Fig. 3(e), indicate that the removal efficiency of BrO_3^- at room temperature was significantly higher than at lower temperatures, suggesting that the reaction is endothermic. However, when the temperature ranged from 25 °C to 35 °C, there was no significant difference in the removal rate. This trend is also consistent with previous research.[47,48]

In laboratory experiments, the composition of the prepared solutions is simple and controllable. However, the components are relatively complex in actual water bodies. HA, as a representative dissolved organic matter (DOM) compound, was chosen to investigate its effect on the degradation of BrO_3^- when in the presence of the 1% Au/TiO_2 photocatalyst. Therefore, it is of great significance to study the effect of dissolved organic matter (DOM) on the photo-reduction of BrO_3^-.[49] Humic acid (HA) was selected to investigate the effect of DOM on the degradation of BrO_3^- by 1% Au/TiO_2 photocatalyst. As shown in Fig. 3(f), the BrO_3^- reduction was significantly inhibited when HA was added to the solution. When the HA concentrations in the system were 0.5, 1.0, 2.0, and 5.0 mg L^{-1}, the BrO_3^- removal at 60 min was reduced to 54%, 36%, 29%, and 25%, respectively. It was reported that HA was readily adsorbed onto the surface of the photocatalyst.[50] In addition, it would form competitive adsorption with BrO_3^- and hinder the absorption of UV light by 1% Au/TiO_2 photocatalyst.[51]

It is well known that oxygen is the primary electron acceptor in most experiments and applications involving TiO_2 photocatalysis. Generally speaking, H_2O_2 is formed for the reduction of O_2 by two electrons *via* reaction (2). To eliminate the competitive relationship between O_2 and BrO_3^- in the UV/1% Au/TiO_2 process, nitrogen was used to purge O_2 out of the reactor to maintain a deoxidated condition during the reaction. In theory, O_2 would compete with BrO_3^- for photo-generated electrons. Thus, it was expected that more BrO_3^- would be reduced in the N_2– atmosphere. However, as shown in Fig. 4(a), BrO_3^- degradation decreased in the absence of O_2 compared with the air-atmospheric reaction. This result could be explained by the reason that BrO_3^- was degraded by the H_2O_2. Khalil *et al.* also found that under an N_2-atmosphere, the photo-reduction of Cr(VI) decreased relative to an O_2 atmosphere in a ZnO photocatalytic system.[52] Therefore, we proposed that the absence of H_2O_2 in the N_2-atmosphere attributed to the decrease of BrO_3^- reduction.

The concentration of photo-generated H_2O_2 in the solution was monitored during the photo-reduction of BrO_3^- under air-equilibration and N_2-atmosphere to verify the proposition. As shown in Fig. 4(b), H_2O_2 concentration in the solution gradually increased and eventually reached 8 μmol L^{-1} under air-equilibration, while under the N_2-atmosphere, the maximum content of H_2O_2 detected was 0.6 μmol L^{-1}. The formation of H_2O_2 in the N_2-atmosphere mainly came from two aspects (reactions (2) and (3)). Considering how BrO_3^- was reduced by

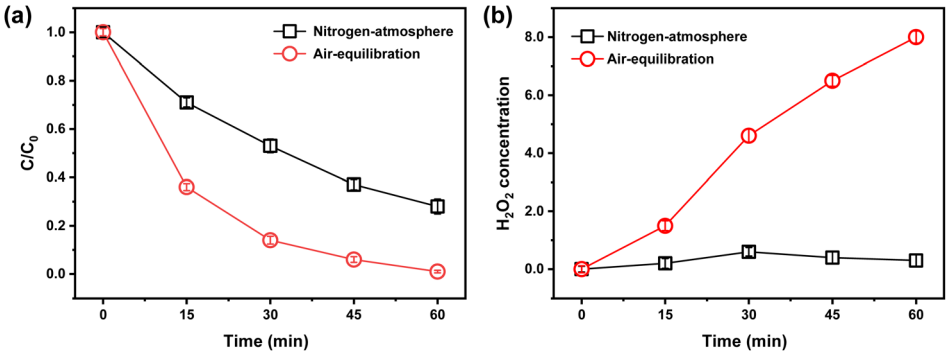

Fig. 4 (a) Comparison of BrO_3^- degradation in nitrogen-atmosphere and air-atmospheric. (b) Various concentrations of H_2O_2 are generated during photo-reduction of BrO_3^- under air-equilibration and nitrogen-atmosphere. Conditions: $[BrO_3^-]_0 = 0.078$ mM (10 mg L^{-1}), 1% Au/TiO_2 dose = 0.3 g L^{-1}, pH = 7.0 ± 0.2, $T = 25 \pm 0.5$ °C, and UV-L light intensity = 2.42 mW cm^{-2}.

H_2O_2, we suggested that BrO^- and BrO_2^- could be reduced to br^- *via* reactions (4) and (5), which was consistent with previous studies.[44] It could be seen that H_2O_2 played an important role in BrO_3^- photo-reduction, which also explained the less degradation of BrO_3^- under the N_2-atmosphere than that under air-equilibration in the UV/1% Au/TiO_2 process.

$$O_2 + 2e^- + H^+ \rightarrow H_2O_2 \quad (2)$$

$$2H_2O + 2h^+ \rightarrow H_2O_2 + 2H^+ \quad (3)$$

$$H_2O_2 + BrO^- \rightarrow Br^- + H_2O + O_2 \quad (4)$$

$$H_2O_2 + BrO_2^- \rightarrow Br^- + H_2O + 2O_2 \quad (5)$$

3.5 Application of UV/1% Au/TiO_2 process in BrO_3^- degradation in tap water

To investigate the BrO_3^- degradation of 1% Au/TiO_2 photocatalyst in practical application, tap water originating from the Yangtze River (Table S1†) and deionized (DI) water were used in this experiment, respectively. As shown in Fig. 5, 1% Au/TiO_2 photocatalyst in both glasses of water demonstrated higher removal efficiency of BrO_3^- than that with UV alone. However, the reduction percentage of BrO_3^- declined to 82% in tap water while almost 100% in DI water after 60 minutes, illustrating an obvious inhibition of BrO_3^- degradation on 1% Au/TiO_2 in tap water. The presence of natural organic matter (NOM) in tap water was identified as the primary factor contributing to the observed effects. NOM has the potential to influence the interaction between the photocatalyst and ultraviolet light, as well as the generation and transfer of photo-generated electrons (e^-). Furthermore, the variation in pH between the two water sources was found to be an additional influential factor, as demonstrated in the previous analysis, affecting the degradation of BrO_3^-. In addition, anions like nitrate in tap water were negatively charged and competed for photo-generated electrons with BrO_3^- in the solution, resulting in a lower reduction of BrO_3^- in the photocatalytic system. Therefore, appropriate treatment could be used to improve the BrO_3^- degradation for natural water, such as the increasing of catalyst dosage, and pretreatment of nitrate and organic matters, which was also what we plan to study in future work.

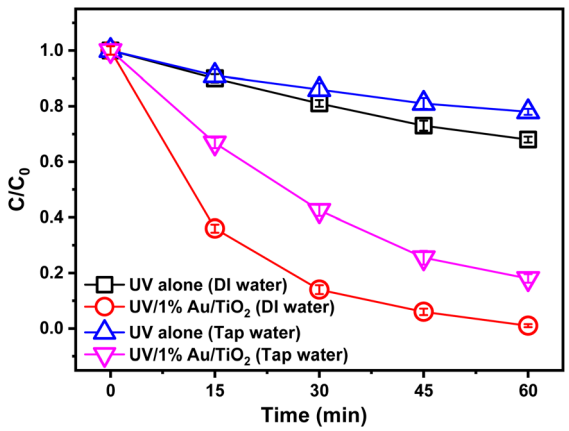

Fig. 5 Comparison of BrO_3^- degradation in tap water treated from Yangtze River and DI water. Conditions: $[BrO_3^-]_0 = 0.078$ mM (10 mg L^{-1}), 1% Au/TiO_2 dosage = 0.3 g L^{-1}, $T = 25 \pm 0.5$ °C, and UV-L light intensity = 2.42 mW cm^{-2}.

3.6 The photocatalytic stability and reusability of 1% Au/TiO_2 photocatalyst

The stability and reusability of photocatalysts are crucial factors for their practical application in water treatment. To assess the stability of the prepared catalyst (1% Au/TiO_2), samples were stored in sealed bottles at a temperature of 20 ± 0.5 °C for different durations (1, 10, 20, 30, and 60 days). As depicted in Fig. 6(a), the percentage of BrO_3^- reduction by the 1% Au/TiO_2 photocatalyst after 60 minutes remained unchanged after 20 days of storage, with a high removal rate of 97% maintained after 30 days of storage. However, after 60 days of storage, the BrO_3^- removal rate at 60 minutes dropped to approximately 95%, which could be attributed to the agglomeration phenomenon caused by moisture absorption and a decrease in photocatalytic performance. Therefore, it is recommended to

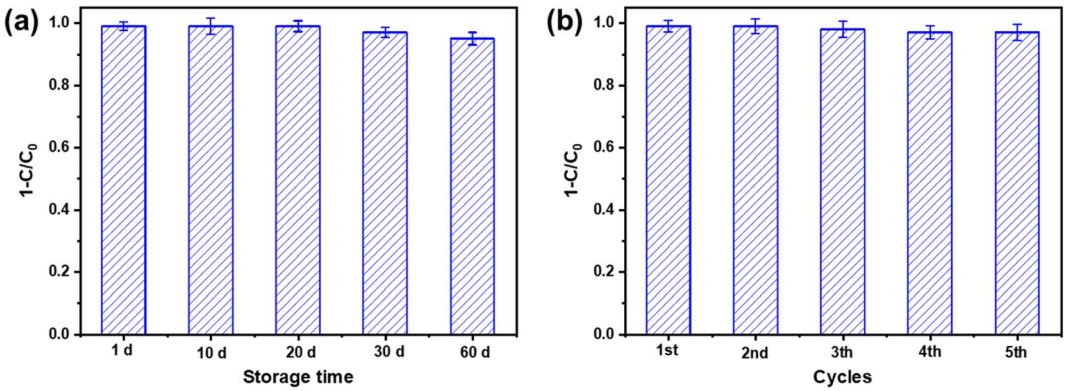

Fig. 6 The BrO_3^- removal ratio by 1% Au/TiO_2 photocatalyst at 60 min when the photocatalyst (a) was stored for a different number of days in glass bottles in the dark at 20 ± 0.5 °C and (b) was used for a different number of cycles of 60 min BrO_3^- degradation experiments. Conditions: $[BrO_3^-]_0 = 0.078$ mM (10 mg L^{-1}), 1% Au/TiO_2 dose = 0.3 g L^{-1}, pH = 7.0 ± 0.2, DO = 8.1 mg L^{-1}, $T = 25 \pm 0.5$ °C, and UV-L light intensity = 2.42 mW cm^{-2}.

store the catalyst in a dry and airtight container with shading treatment to maintain its stability.

Furthermore, the reusability of the photocatalyst was investigated. Fig. 6(b) illustrates the percentage of BrO_3^- reduction by the 1% Au/TiO_2 photocatalyst after five consecutive runs. After each run, the collected catalyst particles were washed with DI water and ethanol and dried at 60 °C in preparation for the next photo-reduction cycle. It can be observed that after five cycles, the efficiency of the photocatalyst was not reduced, indicating that the catalytic activity of the 1% Au/TiO_2 catalyst remained intact under the given reaction conditions, at least for up to five cycles. Additionally, to assess whether the morphology and structure of the catalyst changed after the photocatalytic process, post-reaction characterization of the catalyst was performed. SEM images and XRD patterns were obtained after the reaction. The SEM images (Fig. S6†) showed no significant morphological changes, and the XRD patterns (Fig. S7†) confirmed that the crystalline structure of the catalyst remained unchanged. These characterization further proved the stability of the catalyst in the process of photocatalysis.

3.7 Proposed photo-reduction mechanism by 1% Au/TiO_2 photocatalyst

To investigate the role of electrons in the UV/1% Au/TiO_2 reduction system of BrO_3^-, $K_2S_2O_8$ was chosen to add into the reaction solution as a quencher for electrons, which had been confirmed preferentially reacted with electrons compared to BrO_3^-.[53] The test results are shown in Fig. 7(a). The BrO_3^- degradation decreased significantly with the increase of $K_2S_2O_8$ dosage. BrO_3^- removal decreased with adding 2 mmol l^{-1} $K_2S_2O_8$ and was completely inhibited in the presence of 4 and 6 mmol l^{-1} $K_2S_2O_8$ after 60 minutes. These results indicated that electrons play an indispensable role in BrO_3^- reduction.

Photoluminescence (PL) spectra are commonly used to study the lifetimes of photo-generated electrons and holes of photocatalysts.[54,55] Fig. 7(b) shows the PL spectra of the Au/TiO_2 photocatalyst. In comparison to pure TiO_2, the PL intensity across the entire luminescence wavelength range exhibited a significant decrease upon loading Au onto TiO_2, with the lowest intensity observed for the 1% Au/TiO_2 sample. Upon Au loading, a considerable reduction in PL intensity across the entire range of luminescence wavelengths was observed, with the most notable decrease observed in the case of 1% Au/TiO_2 in comparison to pure TiO_2. Since the work function of Au is larger than that of TiO_2, it forms electron capture traps on the surface of TiO_2, which significantly reduces the complexation of photo-generated electrons and holes and leads to a decrease in the peak of the PL.[56] This phenomenon suggests a restricted occurrence of electron–hole pair complexation following the introduction of Au into the system.

To obtain the transient photo-response of Au/TiO_2 photocatalyst, photocurrent density (PC) was measured in 0.5 M Na_2SO_4 solution with several cycles of 20 s intervals light on or off under illumination. It was found that a larger photocurrent could indicate higher electron and hole separation efficiency.[57] The PC response measurement (Fig. 7(c)) showed that the photo-generation current density of 1% Au/TiO_2 significantly improved compared with that of pure TiO_2. The maximum photocurrent was observed with the 1% Au/TiO_2, which represented that it had the highest photo-generated electron–hole pairs separation efficiency and lowest carrier recombination rate. The excellent photo-electric performance of 1% Au/TiO_2 also demonstrated its potential application in other fields.

In addition, electrochemical impedance spectroscopy (EIS) was measured to investigate the charge transfer efficiency at the surface of the as-prepared working electrodes under light irradiation.[58] As shown in Fig. 7(d), the radius of the semicircle in the EIS spectrum decreased in the order of pure TiO_2 > 5% Au/TiO_2 > 0.5% Au/TiO_2 > 1% Au/TiO_2, indicating that the interfacial charge transfer resistance also decreased in the same order.

The DMPO–ESR was used to analyze further the role of electrons in the UV/Au/TiO_2 reaction system, as previous studies have shown that DMPO could be used as a trapping agent to detect electrons in the solution.[59] As depicted in Fig. 7(e), pure TiO_2 and 1% Au/TiO_2 composites could observe the ESR signal

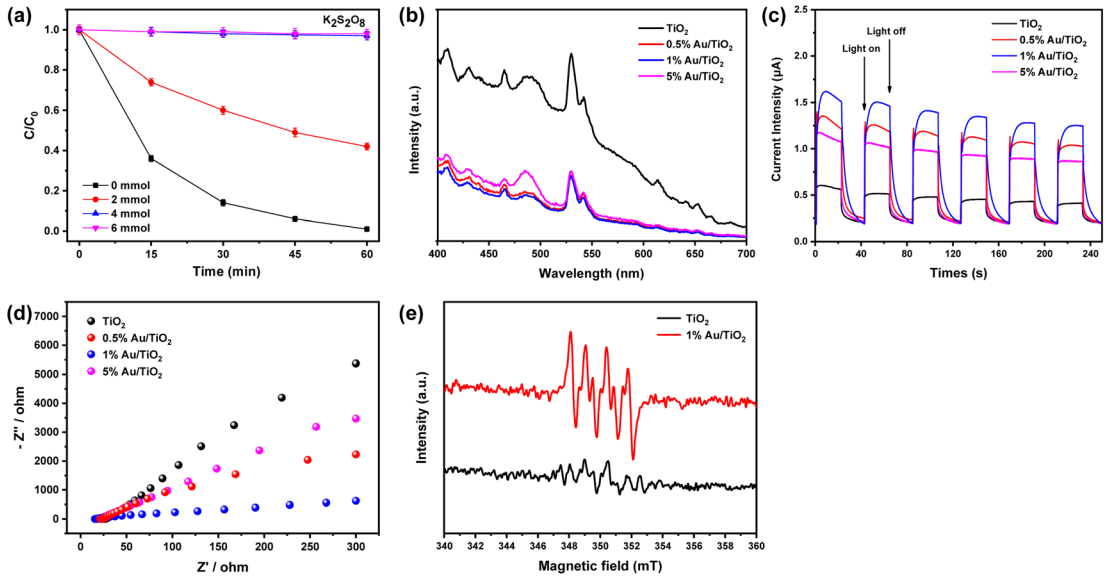

Fig. 7 (a) The effect of $K_2S_2O_8$ on the reduction of BrO_3^- by 1% Au/TiO_2 photocatalyst under ultraviolet light irradiation. (b) PL, (c) PC and (d) EIS spectra of TiO_2 and Au/TiO_2 photocatalyst. (e) DMPO spin-trapping ESR spectra of TiO_2 and 1% Au/TiO_2 photocatalyst in methanol dispersion for DMPO-$^{\bullet}O_2^-$ under UV irradiation.

of $^{\bullet}O_2^-$, corresponding to the characteristic peak spectrum of DMPO-$^{\bullet}O_2^-$. This phenomenon indicated that $^{\bullet}O_2^-$ was produced in the photocatalytic reaction process. Analyzing the signal strength, it could be found that the peak intensity of DMPO-$^{\bullet}O_2^-$ adduct for 1% Au/TiO_2 photocatalyst was much higher than that of pure TiO_2, indicating that after the loading of Au NPs on TiO_2, more electrons were produced.[42] In conclusion, higher BrO_3^- degradation could be observed by 1% Au/TiO_2 photocatalyst to promote the electrons generated in the reduction system.

Therefore, the utilization of Au/TiO_2 photocatalyst in conjunction with UV irradiation results in enhanced separation of electron–hole pairs within TiO_2. This improvement can be attributed to the presence of gold nanoparticles (NPs), which function as electron sinks due to the formation of a Schottky barrier between the metal and the semiconductor. The Au NPs effectively capture photo-generated electrons, acting as electron donors and facilitating the photo-reduction of BrO_3^-.[39] The degradation mechanism of BrO_3^- by the Au/TiO_2 photocatalyst is depicted in Scheme 1. Furthermore, the removal of Br^- in

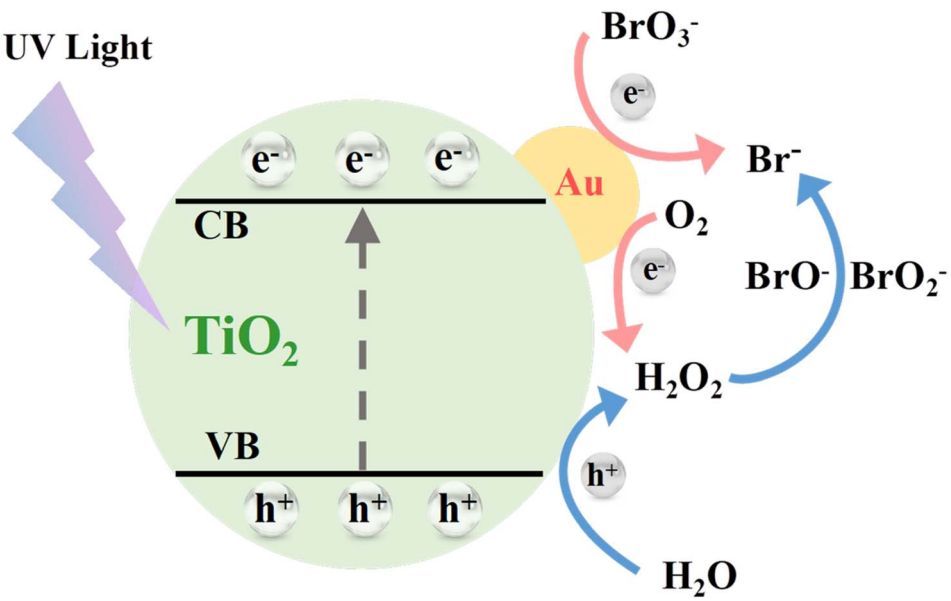

Scheme 1 Schematic of the mechanism of BrO_3^- reduction by Au/TiO_2 photocatalyst under UV irradiation. VB: valence band; CB: conduction band.

addition to BrO_3^- is an important factor that cannot be ignored in practical applications. The feasibility of other removal methods will be explored in detail in future studies.

4 Conclusions

In this study, a novel Au/TiO_2 photocatalyst was prepared by a simple solvothermal one-step method. Compared with pure TiO_2, the TiO_2 composite nanoparticles loaded with Au NPs have higher BrO_3^- removal efficiency. 99% BrO_3^- removal was achieved after 60 minutes at 1% Au and 0.3 g l^{-1} catalyst dosage. The inclusion of Au in the system proved to be a crucial factor in facilitating the photo-reduction of BrO_3^-. Upon UV irradiation, there was a notable migration of photo-generated electrons from the TiO_2 semiconductor towards the Au NPs, thereby enhancing the efficiency of BrO_3^- photo-reduction. Consequently, the Au/TiO_2 photocatalyst demonstrated effective photo-reduction of BrO_3^- under UV light irradiation, eliminating the need for sacrificial agents in the reaction solution. The promising regenerative capability and reusability of the Au/TiO_2 photocatalyst highlight its potential for further development. Moreover, the integration of this new method with UV disinfection holds practical significance, particularly in water treatment facilities. This study not only introduces a novel and efficient photo-reduction process for BrO_3^- removal but also provides insights into the impact of raw water constituents on BrO_3^- treatment, thereby offering valuable guidance in this field.

Data availability

The data underlying this article are available in the article and in its online ESI.†

Author contributions

Ying Xu: data curation, software, formal analysis, writing – original draft, writing – review & editing. Shuili Yu: conceptualization, supervision, resources, funding acquisition. Cong Huang: investigation, visualization, writing – review & editing. Zheng Xu: investigation, funding acquisition, writing – review & editing.

Conflicts of interest

We declare that we have no competing interests that could have influenced the work reported in this paper.

Acknowledgements

The authors gratefully acknowledge financial support from the National Natural Science Foundation of China (No. 52170011) and Zhejiang Province construction research project (No. 2023K177).

References

1 W. W. Yang and T. T. Wu, Evaluation of plasmon-enhanced catalytic ozonation for the abatement of micropollutants in environmental matrices, *Water Res.*, 2022, **211**, 118072.
2 X. Zhao, G. Zhang and Z. Zhang, TiO2-based catalysts for photocatalytic reduction of aqueous oxyanions: State-of-the-art and future prospects, *Environ. Int.*, 2020, **136**, 105453.
3 T. Fujioka, S. Boivin and H. Takeuchi, Online monitoring of bromate in treated wastewater: implications for potable water reuse, *Environ. Sci.: Water Res. Technol.*, 2022, **8**(10), 2034–2039.
4 S. W. Krasner, W. H. Glaze, H. S. Weinberg, *et al.*, Formation and control of bromate during ozonation of waters containing bromide, *J. – Am. Water Works Assoc.*, 1993, **85**(1), 73–81.
5 M. Flury and A. Papritz, Bromide in the Natural Environment: Occurrence and Toxicity, *J. Environ. Qual.*, 1993, **22**(4), 747–758.
6 M. Liu, C. Meng and L. Yuan, Modulation of spatiotemporal dynamics in the bromate-sulfite-ferrocyanide reaction system by visible light, *RSC Adv.*, 2022, **12**(24), 15145–15149.
7 S. S. Tang, J. Yao, H. Y. Liu, *et al.*, Enhancement of photocatalytic bromate reduction by TiO2 coupled with Ti(3)C(2)MXene as efficient non-noble cocatalyst: Performance and mechanism, *J. Environ. Chem. Eng.*, 2022, **10**(1), 107099.
8 W. Zhou, Y. Yang, W.-Z. Gai, *et al.*, A comparative study on high-efficient reduction of bromate in neutral solution using zero-valent Al treated by different procedures, *Sci. Total Environ.*, 2021, **795**, 148786.
9 Y. Xu, Z. W. He, S. L. Yu, *et al.*, Advanced reduction of bromate by UV/TiO2-Bi process without external sacrificial agents: Mechanism and applications, *Chem. Eng. J.*, 2022, **429**, 132104.
10 Q. Xiao, T. Wang, S. L. Yu, *et al.*, Influence of UV lamp, sulfur(IV) concentration, and pH on bromate degradation in UV/sulfite systems: Mechanisms and applications, *Water Res.*, 2017, **111**, 288–296.
11 V. S. V. Botlaguduru, B. Batchelor and A. Abdel-Wahab, Application of UV-sulfite advanced reduction process to bromate removal, *J. Water Proc. engineering*, 2015, **5**, 76–82.
12 A. Kumar, G. Sharma, M. Naushad, *et al.*, Highly visible active Ag2CrO4/Ag/BiFeO3@RGO nano-junction for photoreduction of CO2 and photocatalytic removal of ciprofloxacin and bromate ions: The triggering effect of Ag and RGO, *Chem. Eng. J.*, 2019, **370**, 148–165.
13 K. Y. A. Lin, J. Y. Lin and H. L. Lien, Valorization of aluminum scrap via an acid-washing treatment for reductive removal of toxic bromate from water, *Chemosphere*, 2017, **172**, 325–332.
14 Z. Wu, Y. Tang, W. Li, *et al.*, Formation control of bromate and trihalomethanes during ozonation of bromide-containing water with chemical addition: Hydrogen peroxide or ammonia?, *J. Environ. Sci.*, 2021, **110**, 111–118.

15 J. A. Wisniewski and M. Kabsch-Korbutowicz, Removal of nitrate and bromate ions from water in processes with ion-exchange membranes, *Desalin. Water Treat.*, 2021, **214**, 8–15.
16 G. Gordon, R. D. Gauw, G. L. Emmert, *et al.*, Chemical reduction methods for bromate ion removal, *J. – Am. Water Works Assoc.*, 2002, **94**(2), 91–98.
17 A. Mills, A. Belghazi and D. Rodman, Bromate removal from drinking water by semiconductor photocatalysis, *Water Res.*, 1996, **30**(9), 1973–1978.
18 Y. Zhang, L. Li and H. Liu, Photocatalytic Reduction Activity of {001} TiO2 Codoped with F and Fe under Visible Light for Bromate Removal, *J. Nanomater.*, 2016, **2016**, 5646175.
19 G. Li, X. Li, X. Hao, *et al.*, Ti3+/Ti4+and Co2+/Co3+redox couples in Ce-doped Co-Ce/TiO2 for enhancing photothermocatalytic toluene oxidation, *J. Environ. Sci.*, 2025, **149**, 164–176.
20 E. Kowalska, H. Remita, C. Colbeau-Justin, *et al.*, Modification of titanium dioxide with platinum ions and clusters: Application in photocatalysis, *J. Phys. Chem. C*, 2008, **112**(4), 1124–1131.
21 P. A. Desario, J. J. Pietron, D. E. Devantier, *et al.*, Plasmonic enhancement of visible-light water splitting with Au-TiO2 composite aerogels, *Nanoscale*, 2013, **5**(17), 8073–8083.
22 K. Tada, Y. Maeda, H. Koga, *et al.*, TiO2 Crystal Structure Dependence of Low-temperature CO Oxidation Catalyzed by Au/TiO2, *Chem. Lett.*, 2018, **47**(2), 200–203.
23 Y. Zhou, Y. Zhu, X. Yang, *et al.*, Au decorated Fe3O4@TiO2 magnetic composites with visible light-assisted enhanced catalytic reduction of 4-nitrophenol, *RSC Adv.*, 2015, **5**(62), 50454–50461.
24 X. Liu, T. Lv, Y. Liu, *et al.*, TiO2-Au composite for efficient UV photocatalytic reduction of Cr(VI), *Desalin. Water Treat.*, 2013, **51**(19–21), 3889–3895.
25 Y.-C. Pu, G. Wang, K.-D. Chang, *et al.*, Au Nanostructure-Decorated TiO2 Nanowires Exhibiting Photoactivity Across Entire UV-visible Region for Photoelectrochemical Water Splitting, *Nano Lett.*, 2013, **13**(8), 3817–3823.
26 I. S. Grover, R. C. Prajapat, S. Singh, *et al.*, Highly photoactive Au-TiO2 nanowires for improved photo-degradation of propiconazole fungicide under UV/sunlight irradiation, *Sol. Energy*, 2017, **144**, 612–618.
27 Z. Y. Li, D. Wu, W. B. Gong, *et al.*, Highly Efficient Photocatalytic CO_2 Methanation over Ru-Doped TiO_2 with Tunable Oxygen Vacancies, *Chin. J. Struct. Chem.*, 2022, **41**(12), 2212043–2212050.
28 R. M. Mohamed and I. A. Mkhalid, Visible light photocatalytic degradation of cyanide using Au-TiO2/multi-walled carbon nanotube nanocomposites, *J. Ind. Eng. Chem.*, 2015, **22**, 390–395.
29 O. L. Stroyuk, V. M. Dzhagan, A. V. Kozytskiy, *et al.*, Nanocrystalline TiO_2/Au films: Photocatalytic deposition of gold nanocrystals and plasmonic enhancement of Raman scattering from titania, *Mater. Sci. Semicond. Process.*, 2015, **37**, 3–8.
30 J. Singh and R. K. Soni, Tunable optical properties of Au nanoparticles encapsulated TiO_2 spheres and their improved sunlight mediated photocatalytic activity, *Colloids Surf., A*, 2021, **612**, 126011.
31 M. Abid, S. Bouattour, A. M. Ferraria, *et al.*, Functionalization of cotton fabrics with plasmonic photo-active nanostructured Au-TiO_2 layer, *Carbohydr. Polym.*, 2017, **176**, 336–344.
32 P. Shahini and A. A. Ashkarran, Immobilization of plasmonic Ag-Au NPs on the TiO_2 nanofibers as an efficient visible-light photocatalyst, *Colloids Surf., A*, 2018, **537**, 155–162.
33 J. A. O. Méndez, C. R. López, E. P. Melián, *et al.*, Production of hydrogen by water photo-splitting over commercial and synthesised Au/TiO_2 catalysts, *Appl. Catal., B*, 2014, **147**, 439–452.
34 Y. Liu, F. B. Yu, F. Wang, *et al.*, Construction of Z-Scheme In_2S_3-TiO_2 for CO_2 Reduction under Concentrated Natural Sunlight, *Chin. J. Struct. Chem.*, 2022, **41**(1), 2201034–2201039.
35 T. Wang, Y.-L. Zhang, J.-H. Pan, *et al.*, Hydrothermal reduction of commercial P25 photocatalysts to expand their visible-light response and enhance their performance for photodegrading phenol in high-salinity wastewater, *Appl. Surf. Sci.*, 2019, **480**, 896–904.
36 M. C. Lin, L.-W. Nien, C.-H. Chen, *et al.*, Surface enhanced Raman scattering and localized surface plasmon resonance of nanoscale ultrathin films prepared by atomic layer deposition, *Appl. Phys. Lett.*, 2012, **101**(2), 023112.
37 S. Y. Zhao, S. H. Chen, S. Y. Wang, *et al.*, Composite Au/TiO2 nanoparticles: Synthesis, characterization, and assembly by using potentiostatic technique, *J. Colloid Interface Sci.*, 2000, **221**(2), 161–165.
38 S. K. Khore, S. R. Kadam, S. D. Naik, *et al.*, Solar light active plasmonic Au@ TiO2 nanocomposite with superior photocatalytic performance for H-2 production and pollutant degradation, *New J. Chem.*, 2018, **42**(13), 10958–10968.
39 M. Jimenez-Salcedo, M. Monge and M. Teresa Tena, An organometallic approach for the preparation of Au-TiO2 and Au-g-C3N4 nanohybrids: improving the depletion of paracetamol under visible light, *Photochem. Photobiol. Sci.*, 2022, **21**(3), 337–347.
40 J. Fang, Q. Zhao, C. Fan, *et al.*, Bromate formation from the oxidation of bromide in the UV/chlorine process with low pressure and medium pressure UV lamps, *Chemosphere*, 2017, **183**, 582–588.
41 F. Chen, Q. Yang, C. Niu, *et al.*, Enhanced visible light photocatalytic activity and mechanism of $ZnSn(OH)_6$ nanocubes modified with AgI nanoparticles, *Catal. Commun.*, 2016, **73**, 1–6.
42 F. Chen, Q. Yang, Y. Zhong, *et al.*, Photo-reduction of bromate in drinking water by metallic Ag and reduced graphene oxide (RGO) jointly modified BiVO4 under visible light irradiation, *Water Res.*, 2016, **101**, 555–563.
43 H. Park, Y. Park, W. Kim, *et al.*, Surface modification of TiO2 photocatalyst for environmental applications, *J. Photochem. Photobiol., C*, 2013, **15**, 1–20.

44 U. Von Gunten and Y. Oliveras, Advanced oxidation of bromide-containing waters: Bromate formation mechanisms, *Environ. Sci. Technol.*, 1998, **32**(1), 63–70.

45 J.-C. Sin, S.-M. Lam, A. R. Mohamed, *et al.*, Degrading Endocrine Disrupting Chemicals from Wastewater by TiO2 Photocatalysis: A Review, *Int. J. Photoenergy*, 2012, **2012**, 185159.

46 X. Zhang, T. Zhang, J. Ng, *et al.*, Transformation of Bromine Species in TiO2 Photocatalytic System, *Environ. Sci. Technol.*, 2010, **44**(1), 439–444.

47 Y. Zhang, J. R. Li, L. D. Li, *et al.*, Influence of parameters on the photocatalytic bromate removal by F-graphene-TiO2, *Environ. Technol.*, 2021, **42**(2), 248–256.

48 D. F. S. Morais, R. A. R. Boaventura, F. C. Moreira, *et al.*, Advances in bromate reduction by heterogeneous photocatalysis: The use of a static mixer as photocatalyst support, *Appl. Catal., B*, 2019, **249**, 322–332.

49 G. S. Cunha, S. G. S. Santos, B. M. Souza-Chaves, *et al.*, Removal of bromate from drinking water using a heterogeneous photocatalytic mili-reactor: impact of the reactor material and water matrix, *Environ. Sci. Pollut. Res.*, 2019, **26**(32), 33281–33293.

50 K.-Y. A. Lin, C.-H. Lin, S.-Y. Chen, *et al.*, Enhanced photocatalytic reduction of concentrated bromate in the presence of alcohols, *Chem. Eng. J.*, 2016, **303**, 596–603.

51 S.-L. Ding, X.-K. Wang, W.-Q. Jiang, *et al.*, Photodegradation of the antimicrobial triclocarban in aqueous systems under ultraviolet radiation, *Environ. Sci. Pollut. Res.*, 2013, **20**(5), 3195–3201.

52 L. B. Khalil, W. E. Mourad and M. W. Rophael, Photocatalytic reduction of environmental pollutant Cr(VI) over some semiconductors under UV/visible light illumination, *Appl. Catal., B*, 1998, **17**(3), 267–273.

53 X. Zhao, H. Liu, Y. Shen, *et al.*, Photocatalytic reduction of bromate at C-60 modified Bi2MoO6 under visible light irradiation, *Appl. Catal., B*, 2011, **106**(1–2), 63–68.

54 K. Perumal, S. Shanavas, T. Ahamad, *et al.*, Construction of Ag2CO3/BiOBr/CdS ternary composite photocatalyst with improved visible-light photocatalytic activity on tetracycline molecule degradation, *J. Environ. Sci.*, 2023, **125**, 47–60.

55 C. Zhao, L. Zhou, Z. Zhang, *et al.*, Insight of the Influence of Magnetic-Field Direction on Magneto-Plasmonic Interfaces for Tuning Photocatalytical Performance of Semiconductors, *J. Phys. Chem. Lett.*, 2020, **11**(22), 9931–9937.

56 B. B. Tripathy, M. Behera, H. Rath, *et al.*, Evolution of microstructure and optical properties of TiO2/Au nanocomposite, *Indian J. Pure Appl. Phys.*, 2019, **57**(2), 95–100.

57 H. B. He, Z. Z. Luo and C. L. Yu, Embellish zinc tungstate nanorods with silver chloride nanoparticles for enhanced photocatalytic, antibacterial and antifouling performance, *Colloids Surf., A*, 2021, **613**, 126099.

58 H. B. He, J. D. Li, C. L. Yu, *et al.*, Surface decoration of microdisk-like g-C_3N_4/diatomite with Ag/AgCl nanoparticles for application in Cr(VI) reduction, *Sustainable Mater. Technol.*, 2019, **22**, e00127.

59 F. Dong, Z. W. Zhao, Y. J. Sun, *et al.*, An Advanced Semimetal-Organic Bi Spheres-g-C3N4 Nanohybrid with SPR-Enhanced Visible-Light Photocatalytic Performance for NO Purification, *Environ. Sci. Technol.*, 2015, **49**(20), 12432–12440.